International Journal of Heat and Mass Transfer 111 (2017) 289–298

Contents lists available at ScienceDirect

International Journal of Heat and Mass Transfer

journal homepage: www.elsevier.com/locate/ijhmt

Multi-objective optimization of operating conditions and channel structure for a proton exchange membrane fuel cell

Zhichun Liu *, Xiangbing Zeng, Ya Ge, Jun Shen, Wei Liu *

School of Energy and Power Engineering, Huazhong University of Science and Technology, 430074 Wuhan, China

ARTICLE INFO

Article history:
Received 17 November 2016
Received in revised form 15 February 2017
Accepted 31 March 2017
Available online 7 April 2017

Keywords:
PEMFC stack
Operating condition
Channel structure
Multi-objective optimization

ABSTRACT

In this study, the operating condition (operating temperature, anode pressure, cathode pressure and current density) and channel structure (heights of channel inlet and outlet) of a proton exchange membrane fuel cell (PEMFC) are optimized using multi-objective genetic algorithm. The optimizations of the operating condition and channel structure are based on a PEMFC stack model and a three-dimensional, steady-state, non-isothermal PEMFC model, respectively. The optimal operating condition and channel structure are selected by TOPSIS (Technique for Order Preference by Similarity to an Ideal Solution) from the optimal solution set called Pareto front. After the optimized operating condition is obtained, it is applied to the optimization of the channel structure. The results present that the optimal channel structure under the optimal operating condition is a type of tapered channel. Compared to the conventional straight channel, the tapered channel can enhance gas reactant transport in the PEMFC and a greater amount of reactant can participate in the electrochemical reaction, thus, more output power can be obtained.

1. Introduction

The proton exchange membrane fuel cell (PEMFC) is considered as a promising energy conversion device due to their high energy efficiency and low emission [1]. The PEMFC has application prospect in the field of automobile and electronics. However, there exists challenging problems such as high cost of catalyst and low durability that cause difficulties in the wide spread application of the PEMFC [2,3]. Therefore the performance of PEMFC should be improved. During the past decades, many researchers have made efforts to optimize the performance of PEMFC. The optimization of PEMFC can be carried out from two aspects: operating condition and geometric structure.

For optimization of the operating condition, many research efforts have been conducted. Na and Gou [4] set the operating condition as variable to optimize the efficiency and cost of the fuel cell stack by using a multi-objective optimization technique called, the sequential quadratic programming (SQP) method. They discussed the effects of the initial operating condition on the efficiency and cost of the fuel cell stack. Ang et al. [5] developed the PEMFC stack model and optimized the efficiency and the size of the PEMFC stack by using a multi-objective method. The results indicated that when the PEMFC stack operated at an efficiency between 40% and 47% and the membrane electrode assembly (MEA) area was at least 3 cm^2/W, the efficiency and size of PEMFC stack could be balanced and the comprehensive performance of PEMFC stack achieved optimum. In their paper, the results of optimization were selected artificially from the optimal solution set called Pareto front obtained by multi-objective genetic algorithm. Therefore their results were approximate, not exact.

Mert et al. [6] analyzed the energy and exergy efficiencies and power output of the stack at different operating conditions. The operating condition that they took into account included temperature, pressure, anode stoichiometry, and cathode stoichiometry. They found that the temperature and pressure were the positive parameters for the stack efficiency, while the anode and cathode stoichiometry were the negative parameters. Wishart et al. [7] optimized the performance of PEMFC based on a semi-empirical fuel cell stack model from two aspects: net system power and system exergetic efficiency. They used global and local optimization algorithm to optimize the operating condition of PEMFC, respectively and compared the results of these two optimization algorithm. The results showed the optimal operating conditions obtained by global and local optimization algorithm were similar. Mert et al. [8] investigated the effects of operating condition on the PEMFC stack performance by using parametric studies. The results they obtained were identical to the study of Ref. [6].

* Corresponding authors.
E-mail addresses: zcliu@hust.edu.cn (Z. Liu), w_liu@hust.edu.cn (W. Liu).

http://dx.doi.org/10.1016/j.ijheatmasstransfer.2017.03.120
0017-9310/

Nomenclature

A	active area (cm^2)
C	molar concentration (mol/m^3)
D	mass diffusivity of species (m^2/s)
F	Faraday's number 96,487 (C/mol)
i	current (A)
I	current density (A/cm^2)
P	pressure (Pa)
PEMFC	proton exchange membrane fuel cell
R	resistance (Ω) or universal gas constant 8.314 (J/mol K)
T	temperature (K)
T_e	entry air temperature (K)
n_{cell}	number of fuel cells in stack
t	thickness (cm)
$\mathbf{u}$	velocity (m/s)
k	thermal conductivity (W/m K)
K	permeability (m^2)
GA	genetic algorithm
M	molecular weight (g/mol)
MEA	membrane electrode assembly
RH	relative humidity
LHV	lower heating value of hydrogen (2.4×105 J/mol)

Greek letters

α	transfer coefficient
ε	porosity
μ	viscosity (Pa/s)
ρ	density (kg/m^3)
σ	conductivity (S/m)
ϕ	phase potential (V)
ω	species mass fraction
λ	stoichiometric ratio or water content

Subscript

a	anode
c	cathode
ch	channel
M	membrane
obj	objective
ref	reference
mom	momentum
eff	effective
agg	agglomerate
prs	parasitic

Jiao et al. [9] applied a different back pressure to each channel based on a PEM fuel cell with the novel parallel flow channel design. They found that the distributions of reactants were more uniform in the catalyst layer by increasing the pressure difference between the channels. Wan et al. [10] studied the temperature distribution of the PEMFC stack under the different operating conditions with in-situ measurement technology. Their results indicated that the temperature was more uniform as well as exhibiting better performance and generation of less waste heat when the operating pressure increased. Many other researchers [11–13] also studied the performance of the PEMFC under the different operating conditions through the experiment or calculation.

For the optimization of the geometric structure, the channel structure was optimized in many research efforts. Perng et al. [14] installed the transverse rectangular cylinder in the gas flow channel to enhance the performance of a PEMFC. They studied the effect of different gap sizes and the width of the cylinder on the PEMFC performance. Manso et al. [15] established a PEM fuel cell model with a serpentine flow field design and changed the channel cross-section aspect ratio which was defined as the ratio height/width of the channel to improve the cell performance. As a result, a higher channel cross-section aspect ratio provided better performance.

Bilgili et al. [16] installed obstacles in the gas channels to decrease the concentration losses. They found that the obstacles could improve the transport of reactants from channel to gas diffusion layer and made the PEM fuel cell perform better. Yang et al. [17] optimized the channel and rib widths and channel height by using a genetic algorithm to obtain the maximum output power of fuel cell. In their study, when the channel-to-rib width and the channel height were 1.84:1 and 0.515 mm, respectively, the output power of PEMFC would be maximum. Chiu et al. [18] aimed to make the PEMFC obtain higher output power by changing the widths, heights, and aspect ratios of the channel. Their results indicated that decreasing the channel cross-section could enhance gas velocity so that better performance was obtained.

Perng and Wu [19] proposed a tapered channel with a baffle plate to improve the performance of a fuel cell and optimized the structure of the baffle plate by applying an element-by-element preconditioned conjugate gradient method. The parameters of tapered ratio and gap ratio were the optimization variables while the cell performance was the objective function in their study. They found that a tapered flow channel with a baffle plate improved the fuel cell performance because of better gas transport performance. However, the high pressure loss caused by a tapered flow channel and baffle blockage was not considered in their work as that would have increased the balance of plant (BOP) power consumption.

Hasan et al. [20] simulated a PEMFC by using a three-dimensional, non-isothermal model with rectangular, trapezoidal and parallelogram channel cross-sections. The results showed that the rectangular channel cross-section showed better output performance. But the trapezoidal channel cross-section resulted in more even distributions of reactant and current density. Perng et al. [21] analyzed the fuel cell performance enhancement on changing the catalyst surface layer to a protuberance-like form. They found that the ribs opposite the protuberances enhanced gas reactant transport in the channel of the PEMFC, thereby improving cell performance. Kuo et al. [22] proposed a gas flow channel based on three novel periodic patterns geometries. These three kinds of channels improved the heat and mass transfer performance that led to better electrochemical reaction performance of a PEMFC. Jang et al. [23] designed baffles into flow channels of a fuel cell and optimized the baffles locations for obtaining maximum average current density by the method of combining the simplified conjugate-gradient method and commercial CFD code. Other researchers [24–26] also proposed some improved channel structure for enhancing the performance of PEMFC.

In summary, in the previous researches, combining the multi-objective optimization algorithm and TOPSIS selection for finding the optimal operating condition of fuel cell is rarely found. And introducing the multi-objective optimization algorithm into channel structure optimization to find a global optimal solution appeared unusually in the past studies. In this work, we combine the optimizations of operating condition and channel structure and optimize the operating condition and channel structure of fuel cell by multi-objective genetic algorithm. And TOPSIS is used for selecting optimal operating condition and channel structure from Pareto front obtained by multi-objective genetic algorithm.

2. PEMFC stack model

There are a series of equations to describe a fuel cell stack model [7]. The equations are as follows:

$$V_{cell} = E_{Nernst} - V_{act} - V_{ohmic} - V_{con} \tag{1}$$

In above equation, V_{cell} is the voltage of the fuel cell, E_{Nernst} is the Nernst voltage, V_{act} is the activation overvoltage, V_{ohmic} is the ohmic overvoltage, and V_{con} is the concentration overvoltage. The expressions of each term in above equation can then be defined as follows:

$$E_{Nernst} = 1.229 - 0.85 \times 10^{-3}(T - 298.15) + 4.3085 \times 10^{-5} T \times \left(\ln(P_{H_2}) + \frac{1}{2}\ln(P_{O_2})\right) \tag{2}$$

$$V_{act} = -[\xi_1 + \xi_2 T + \xi_3 T \ln(C_{O_2}) + \xi_4 T \ln(i)] \tag{3}$$

$$V_{ohmic} = i(R_M + R_C) \tag{4}$$

$$V_{con} = -b\ln\left(1 - \frac{I}{I_{max}}\right) \tag{5}$$

The expressions of the parameters in Eqs. (2)–(5) are summarized in Table 1.

The parameters ξ_k (k = 1, 2, 3, 4) are the parametric coefficients of the PEM fuel cell model. These four parameters stand for flow transportation, heat conduction, and the dynamic electrochemical reaction, respectively. The value b is a parametric coefficient (V). R_C is the contact resistance, and I_{max} is the maximum current density [27]. For different PEM fuel cells, the parameters mentioned above are different. In order to make the PEM fuel cell stack model reliable, in this work, we apply a genetic algorithm (GA) to estimate the seven parameters (ξ_1, ξ_2, ξ_3, ξ_4, b, R_C, I_{max}) for fitting polar curve of model and experiment. Here, the sum of the squared of the difference between the output voltages of the PEM fuel cell stack model and output voltages of experiment is used to be the objective function [27]:

$$f_{obj} = \min\left(\sum_{i=1}^{M}(V_s - V_{sm})^2\right) \tag{6}$$

where V_s is the voltage of PEMFC stack model and V_{sm} is the experiment output voltage. When the objective function achieves the minimum value, the optimal parameters are obtained.

As shown in Fig. 1, the results of the PEMFC stack model with optimal parameters are in good agreement with the experimental data [28]. The optimal values of ξ_1, ξ_2, ξ_3, ξ_4, b, R_C, I_{max} are shown in Table 2 and minimum value of objective function f_{obj} is 0.0103. It represents that the PEMFC stack is reliable when those seven parameters achieved optimum. Therefore, this model with optimal parameters is used as the basic model for the multi-objective optimization of the operating condition in the next section.

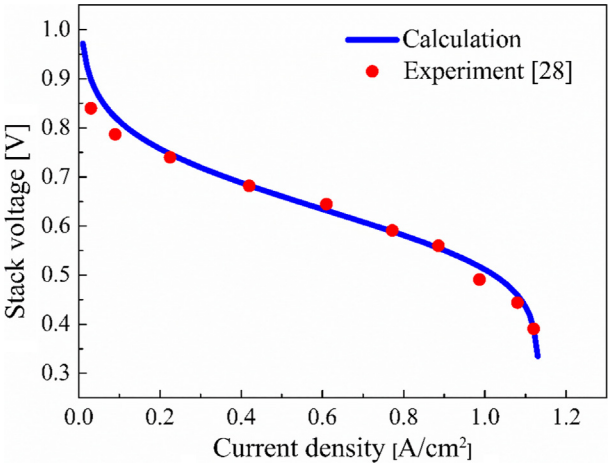

Fig. 1. The polar curve of the stack model with optimal parameters and experimental data.

3. Multi-objective optimization of the operating condition

3.1. Evaluation criterions of the PEMFC stack

Based on the PEMFC stack model mentioned above, the method of the multi-objective optimization is applied to optimize the performance of the PEMFC stack. There are two key evaluation criterions, which are the output power and energy efficiency of the stack. The expressions of the output power and energy efficiency are defined as follows [5]:

$$W_{stack} = n_{cell} A I V_{cell} \tag{7}$$

$$\eta = \frac{W_{stack} - W_{prs}}{W_{fuel}} \tag{8}$$

In Eqs. (7) and (8), η is the energy efficiency of the fuel cell stack. W_{stack} is the output power of the fuel cell stack, W_{prs} is the parasitic power that includes the power consumption of compressor and other power losses and W_{fuel} is power inherent in the fuel. They can be described by the following equations.

$$W_{prs} = W_{comp} + W_{others} \tag{9}$$

$$W_{comp} = \frac{c_p T_e}{\eta_c \eta_{mt}}\left[\left(\frac{P}{P_{in}}\right)^{0.286} - 1\right] m_{air} \tag{10}$$

$$m_{air} = 3.57 \times 10^{-7} \lambda_{air} n_{cell} I A \tag{11}$$

$$W_{others} = 0.05 W_{stack} \tag{12}$$

Table 1
Expressions of the parameters for PEMFC stack.

Description	Equation
Effective partial pressure of hydrogen	$P_{H_2} = 0.5RH_a P^{sat}_{H_2O}\left[\left(\exp\left(\frac{1.635(i/A)}{T^{1.334}}\right) \times \frac{RH_a P^{sat}_{H_2O}}{P_a}\right)^{-1}\right] - 1$
Effective partial pressure of oxygen	$P_{O_2} = P_c\left[1 - x^{sat}_{H_2O} - x_{other\ gases}\exp(0.291 i/T^{0.832})\right]$
Saturation pressure of water vapor	$\log_{10}(P^{sat}_{H_2O}) = 2.95 \times 10^{-2}(T - 273.15) - 9.18 \times 10^{-5}(T - 273.15)^2 + 1.4 \times 10^{-7}(T - 2.1573)^3 - 2.18$
Concentration of dissolved oxygen	$C_{O_2} = P_{O_2}/(5.08 \times 10^6 \exp(-498/T))$
The equivalent resistance of the membrane	$R_M = \frac{\rho_M t_M}{A}$
Specific resistively of the membrane for the electron flow	$\rho_M = \frac{181.6\left[1 + 0.03\left(\frac{i}{A}\right) + 0.062\left(\frac{T}{303}\right)^2\left(\frac{i}{A}\right)^{2.5}\right]}{\left[\lambda - 0.634 - 3\left(\frac{i}{A}\right)\right]\exp\left[4.18\left(\frac{T-303}{T}\right)\right]}$

Table 2
Optimal values of the PEMFC model parameters.

Model parameters	ξ_1	ξ_2	ξ_3	ξ_4	b	R_C	I_{max}	f_{obj}
Optimal value	−0.9496	3.2486e−3	7.4925e−5	−1.8801e−4	0.0461	1.0001e−4	1.1341	0.0103

$$W_{fuel} = \lambda_{H_2} n_{cell} \frac{IA}{2F} \mathrm{LHV} \tag{13}$$

In Eq. (9), W_{comp} is the power consumption of the compressor and W_{others} represents the other power losses. According to Ref. [5], W_{others} is set to 5% of the nominal stack output power.

The energy efficiency and output power of the basic model are calculated. As shown in Fig. 2, the energy efficiency and the output power display different tendencies with the change of current density. If the PEMFC stack achieves a high energy efficiency, the output power will be low, and vice versa. It can be seen that the energy efficiency and output power are two conflicting objectives. Hence, a trade-off between energy efficiency and output power exists. Appropriate energy efficiency and output power are important for the PEMFC stack. Therefore, the resolution of a multi-objective optimization problem for optimizing the performance of the PEMFC stack is required.

3.2. Optimization method

In this work, the MATLAB genetic algorithm toolbox is used to solve the multi-objective optimization problem. The multi-objective optimization problem can be described by the following mathematic model [29].

$$\min[f_1(x), f_2(x), \ldots, f_m(x)] \tag{14}$$

$$\text{s.t.} \begin{cases} lb \leqslant x \leqslant ub \\ Aeq * x = beq \quad x = (x_1, x_2, \ldots, x_n)^{\mathrm{T}} \\ A * x \leqslant b \end{cases}$$

where $f_i(x)$ $(i = 1,2,\ldots,m)$ are the objective functions, x represents the variable, lb and ub are the lower limit and upper limit of x, and $Aeq * x \leqslant beq$ and $A * x \leqslant b$ are the linear equality constraint and linear inequality constraint of x. Here, the aim of multi-optimization is achieving a minimum of the all objective functions $f_i(x)$. However the objective functions are often in conflict with each other, which implies that no single optimum solution can make all the objective functions achieve the minimum value simultaneously. Therefore, there exist many solutions that enable the objective functions to be optimal. These solutions are represented by a set of points and such points form the Pareto front. The Pareto front represents the optimal solutions of multi-optimization problem. The procedure of the multi-objective optimization is shown in Fig. 3.

In this work, the negatives of the energy efficiency, η and output power, W_{stack} are chosen to be the objective functions. The variables are the parameters of the stack's operating conditions which are temperature, T, anode pressure, P_a, cathode pressure, P_c, and current density, I. Therefore, the mathematic model mentioned above is:

$$\min[-\eta, -W_{stack}] \tag{15}$$

s.t.

$323 \leqslant T \leqslant 363.15$ K
$1.1 \leqslant P_a \leqslant 5$ atm
$1.1 \leqslant P_c \leqslant 5$ atm
$0.3 \leqslant I \leqslant 1.3$ A/cm^2

3.3. Results of the multi-optimization problem

Fig. 4 provides the optimal solutions of the above multi-optimization problem. In Fig. 4, the axes are energy efficiency and output power while the curve that consists of a set of points represents the Pareto front. The left endpoint of the curve corresponds to the single-optimization problem of maximizing the energy efficiency, which also means the minimum of the output power of the stack. Conversely, the right endpoint of the curve represents the maximum of the output power and minimum of the energy efficiency. These two points do not satisfy the multi-

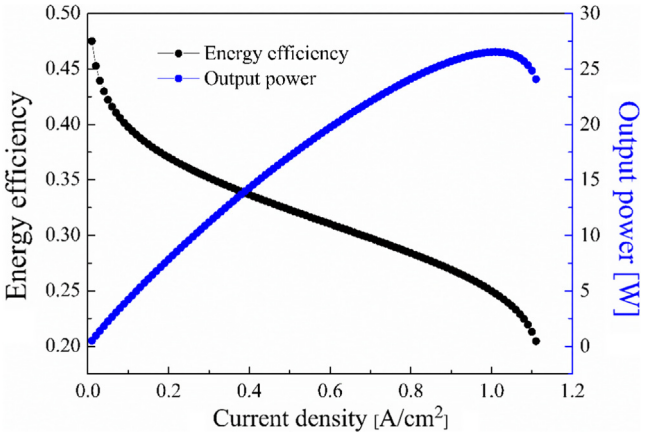

Fig. 2. The energy efficiency and output power of the basic model.

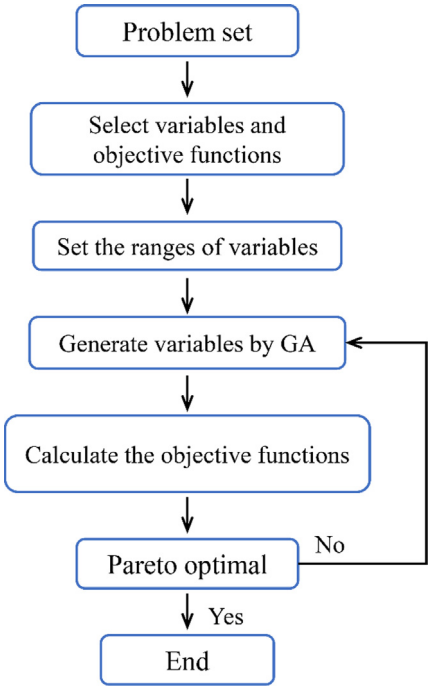

Fig. 3. Flow chart of the optimization process by GA.

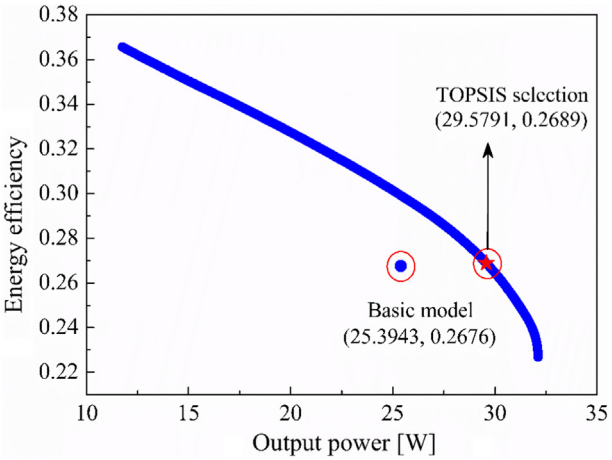

Fig. 4. Pareto front of multi-objective optimization for PEMFC stack.

optimization of the PEMFC stack's performance. The optimal trade-off between the energy efficiency and output power needs to be determined.

In this work, the optimal trade-off between the energy efficiency and output power is chosen by TOPSIS, which is a technique for order preference by similarity to the ideal solution. The basic principle of TOPSIS is to sort through the distance between the evaluation object and the optimal solution and the worst solution, if the evaluation object is closest to the optimal solution and furthest from the worst solution, then it is the best, otherwise it is not the best. TOPSIS is an effective method that can find the optimal trade-off in multi-optimization problem. The TOPSIS process is carried out as follows:

Step 1: Create an evaluation matrix $(x_{ij})_{m\times n}$ consisting of m alternatives and n objectives.

Step 2: The matrix $(x_{ij})_{m\times n}$ is normalized to form the matrix $(r_{ij})_{m\times n}$ by applying the equation below:

$$r_{ij} = \frac{x_{ij}}{\sqrt{\sum_{i=1}^{m} x_{ij}^2}}, \quad i = 1,2,\ldots,m,\ j = 1,2,\ldots,n \tag{16}$$

Step 3: Calculate the weighted normalized matrix $(a_{ij})_{m\times n}$:

$$a_{ij} = w_j \times r_{ij}, \quad i = 1,2,\ldots,m,\ j = 1,2,\ldots,n \tag{17}$$

Step 4: Determine the positive ideal alternative A^+ and the negative ideal alternative A^-:

$$A^+ = (\min[a_{11},\ldots a_{m1}], \min[a_{12},\ldots a_{m2}],\ldots,\min[a_{1n},\ldots a_{mn}]) \tag{18}$$

$$A^- = (\max[a_{11},\ldots a_{m1}], \max[a_{12},\ldots a_{m2}],\ldots,\max[a_{1n},\ldots a_{mn}]) \tag{19}$$

Step 5: Calculate the distance between the target alternative and the positive ideal alternative A^+:

$$d_i^+ = \sqrt{\sum_{j=1}^{n}(a_{ij} - A_j^+)^2}, \quad i = 1,2,\ldots,m,\ j = 1,2,\ldots,n \tag{20}$$

and the distance between the target alternative and the positive ideal alternative A^-:

$$d_i^- = \sqrt{\sum_{j=1}^{n}(a_{ij} - A_j^-)^2}, \quad i = 1,2,\ldots,m,\ j = 1,2,\ldots,n \tag{21}$$

Step 6: Calculate the relative closeness to the ideal solution of alternatives:

$$C_i = \frac{d_i^+}{d_i^+ + d_i^-}, \quad i = 1,2,\ldots,m \tag{22}$$

Step 7: Rank the alternatives according to the value of C_i. The alternative corresponding to the minimum value of C_i is optimal solution.

As can be seen from Fig. 4, the optimal point chosen from the Pareto front by TOPSIS represents the optimized output power and energy efficiency values of 29.5791 W and 0.2689, respectively. Additionally, the optimal operating condition of stack is shown in Table 3.

For comparison, Table 3 provides the operating condition of the basic model which are described in the previous section. The energy efficiency and output power of the basic model are shown in Fig. 4. It can be seen that the optimal model shows the higher output power and higher energy efficiency with respective to the basic model. From Table 3, we can determine that the higher operating temperature and higher pressure of the stack will obtain higher performance. However, when the cathode pressure increases, the parasitic power of the stack will increase. Therefore, the cathode pressure should be lower than the anode pressure to achieve optimization.

4. Optimization of the channel structure

During the multi-objective optimization of the PEMFC stack, the internal structure of PEMFC is not involved. Therefore, the optimal operating condition, as determined from the multi-optimization process above, can be applied to any internal structure of PEMFC. In this section, the structure of PEMFC channel will be optimized under the optimal operating condition by applying the method of the combination of numerical calculation and multi-objective genetic algorithm.

4.1. Model development

4.1.1. Governing equations

To optimize the structure of the PEMFC channel, a three-dimensional, steady-state and non-isothermal model is developed. The geometric structure of the model is shown in Fig. 5. The geometric parameters are listed in Table 4. The governing equations of the model consist of the following equations:

Mass equation

$$\nabla\cdot(\rho\mathbf{u}) = S_{\mathrm{m}} \tag{23}$$

Momentum equation

$$\frac{1}{\varepsilon^2}\nabla\cdot(\rho\mathbf{u}\mathbf{u}) = -\nabla P + \frac{1}{\varepsilon}\nabla\cdot(\mu\nabla\mathbf{u}) + S_{\mathrm{mom}} \tag{24}$$

Energy equation

$$\rho C_{\mathrm{p}}\mathbf{u}\cdot\nabla T = \nabla\cdot(k_{\mathrm{eff}}\nabla T) + S_T \tag{25}$$

Diffusion equation

$$\nabla\cdot\left[-\rho\omega_{\mathrm{i}}\sum_{\mathrm{j}=1}^{N} D_{\mathrm{ij,eff}}\left\{\frac{M}{M_{\mathrm{j}}}\left(\nabla\omega_{\mathrm{j}} + \omega_{\mathrm{j}}\frac{\nabla M}{M}\right) + (x_{\mathrm{j}} - \omega_{\mathrm{j}})\frac{\nabla P}{P}\right\}\right] + \rho\mathbf{u}\cdot\nabla\omega_{\mathrm{i}} = S_{\mathrm{i}} \tag{26}$$

where i is H_2, O_2, or H_2O.

Water content in membrane

Table 3
Results of the operating condition optimization.

Parameters	Temperature (T)	Anode pressure (P_a)	Cathode pressure (P_c)	Current density (I)
Optimal model	366.12 K	4.99 atm	3.02 atm	0.89 A/cm^2
Basic model	343.15 K	1 atm	1 atm	0.89 A/cm^2

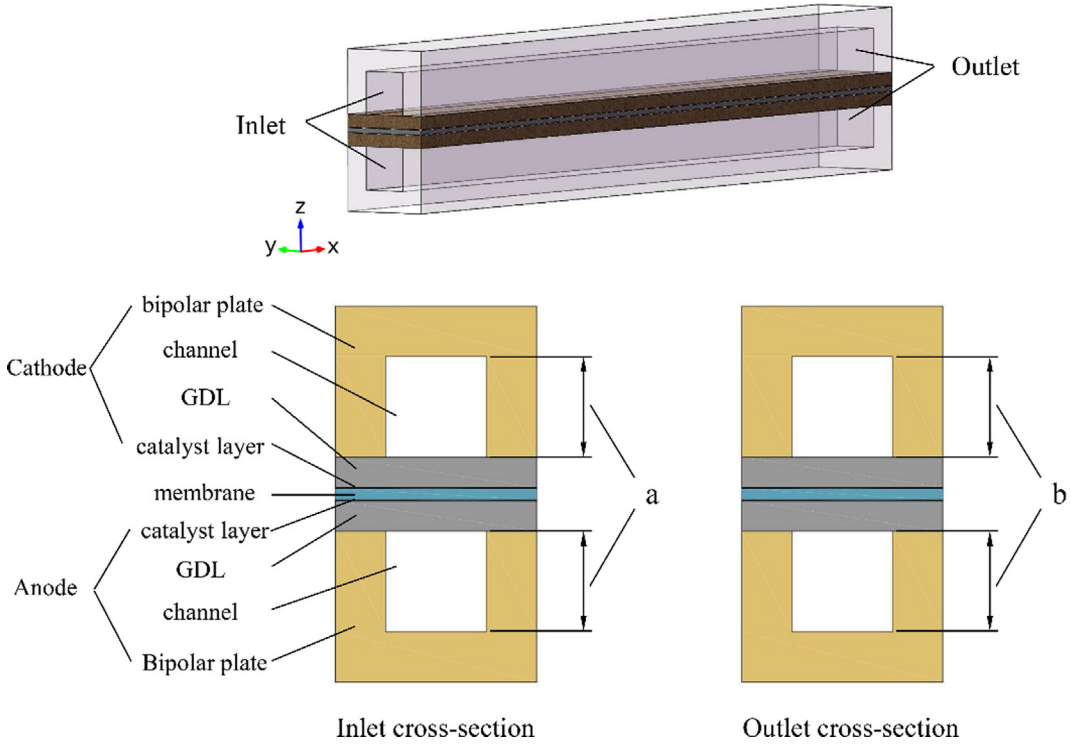

Fig. 5. Geometric structure of a PEMFC model.

Table 4
Geometric parameters.

Parameters	Value [m]
Cell width	2.0×10^{-3}
Channel length	0.02
Channel height	1.0×10^{-3}
Channel width	1.0×10^{-3}
Rib width	1.0×10^{-3}
GDL thickness	0.3×10^{-3}
Catalyst layer thickness	1.29×10^{-5}
Membrane thickness	0.108×10^{-3}

$$\nabla \cdot (D_\lambda \nabla \lambda) + S_\lambda = 0 \tag{27}$$

Conversation of charge

$$\nabla \cdot (\sigma_s \nabla \phi_s) = S_{es} \tag{28}$$

$$\nabla \cdot (\sigma_m \nabla \phi_m) = S_{em} \tag{29}$$

For the solution of the transfer current, the agglomerate model is adopted. The agglomerate model can be described by the following equations.

$$R_{i,eff} = \eta_{agg} R_i \tag{30}$$

$$\eta_{agg} = \frac{3}{\phi_L}\left(\frac{1}{\tanh(\phi_L)} - \frac{1}{\phi_L}\right) \tag{31}$$

$$\phi_L = L_{agg}\sqrt{\frac{|R_i|}{C_i D_i^m}} \tag{32}$$

$$R_i = R_{i,ref}\left(\frac{C_k}{C_{k,ref}}\right)^{\gamma_i}\left(\exp\left(\frac{\alpha_a F}{RT}\eta_i\right) - \exp\left(\frac{\alpha_c F}{RT}\eta_i\right)\right) \tag{33}$$

where i can be a or c representing anode and cathode and k is hydrogen or oxygen.

The source terms and related parameters of Eqs. (23)–(29) are summarized in Table 5.

4.1.2. Boundary conditions

At the anode and cathode inlets as shown in Fig. 5, temperatures, species mass fractions and inlet velocities are specified as follows:

$$\text{Anode inlet}: \quad T_{in,a} = 343\text{K}, \quad u_{in,a} = \zeta_a \frac{i_{max}}{2F} A_m \frac{1}{\omega_{H_2,in}} \frac{RT_{in,a}}{p_{in,a}} \frac{1}{A_{ch}}, \quad \omega_i = \omega_{i,in} \tag{34}$$

$$\text{Cathode inlet}: \quad T_{in,c} = 343\text{K}, \quad u_{in,c} = \zeta_c \frac{i_{max}}{4F} A_m \frac{1}{\omega_{O_2,in}} \frac{RT_{in,c}}{p_{in,c}} \frac{1}{A_{ch}}, \quad \omega_i = \omega_{i,in} \tag{35}$$

In Eqs. (34) and (35), i_{max} is the maximum average current density, A_m is the geometrical area of the membrane, A_{ch} is the channel cross-section area and ω_i is the species mass fraction.

At the anode and cathode outlets, the pressures are set to be the operating pressure. The gradients for other variables are prescribed as zero.

In the y direction, the symmetry boundary conditions are applied. In the z direction, the voltages are prescribed at the sur-

Table 5
Source terms and related parameters of PEMFC model.

Description	Expression
Source terms	$S_m = -\frac{M_{H_2}}{2F}R_{a,eff} - \frac{n_d M_{H_2O}}{F}R_{a,eff}$ (*anode catalyst layer*) $S_m = -\frac{M_{O_2}}{4F}R_{c,eff} + \frac{n_d M_{H_2O}}{F}R_{c,eff} + \frac{M_{H_2O}}{2F}R_{c,eff}$ (*cathode catalyst layer*) $S_{mom} = -\frac{\mu}{K}u$ (*GDL and catalyst layer*) $S_T = \frac{I^2}{\sigma_s}$ (*current collector*) $S_T = \frac{I^2}{\sigma_s^{eff}}$ (*GDL*) $S_T = \frac{I^2}{\sigma_m^{eff}}$ (*membrane*) $S_T = \eta R_i + I^2\left(\frac{1}{\sigma_s^{eff}} + \frac{1}{\sigma_m^{eff}}\right)$ (*catalyst layer*) $S_{H_2} = -\frac{M_{H_2}}{2F}R_{a,eff}$ $S_{O_2} = -\frac{M_{O_2}}{4F}R_{c,eff}$ $S_{H_2O} = \frac{M_{H_2O}}{2F}R_{c,eff}$ $S_{es} = -R_a$; $S_{em} = R_a$ (*anode catalyst layer*) $S_{es} = R_c$; $S_{em} = -R_c$ (*cathode catalyst layer*)
Effective binary diffusivity	$D_{ij,eff} = \varepsilon^{1.5} D_{ij,ref}\left(\frac{P_0}{P}\right)\left(\frac{T}{T_0}\right)^{1.5}$
Water activity	$\alpha = \frac{C_w RT}{P^{sat}_{H_2O}}$
Membrane water diffusivity	$D_w^m = \begin{cases} 3.1\times10^{-7}\lambda(e^{0.28\lambda}-1)e^{(-2346/T)} & 0<\lambda\leqslant 3 \\ 4.17\times10^{-8}\lambda(1+161e^{-\lambda})e^{(-2346/T)} & otherwise \end{cases}$
Water content diffusivity	$D_\lambda = \frac{\rho_m}{EW} D_w^m$
Proton conductivity	$\sigma_m = (0.5139\lambda - 0.326)\exp[1268(\frac{1}{303} - \frac{1}{T})]$.

faces of the anode and cathode bipolar plates. At the anode side, the voltage is set to be zero. At the cathode side, the voltage varies from 0.9 V to 0.4 V with a step of 0.05 V.

4.1.3. Numerical method

The governing equations in Section 4.1.1 are coupled with each other. The finite element method is used to solve those governing equations in COMSOL Multiphysics 5.0 by employing segregated solvers. For the solutions of governing equations, the following physics application modes in COMSOL Multiphysics 5.0 are involved:

- Secondary current distribution for charge conversion equations.
- Reacting flow for mass, momentum and diffusion equations.
- Heat transfer for energy equation.
- General PDE form for water content in membrane.

To examine the grid independence, three grids with 39,900, 57,000 and 73,200 elements are employed. As shown in Fig. 6, the current densities of three grids under the operating voltage of 0.5 V are 0.9569, 0.9528 and 0.95186, respectively. The differences between the grids with 57,000 and 73,200 elements are 0.01%. Therefore, the grid with 57,000 elements is chosen for the simulation. The simulation for each operating voltage or operating current density requires about 10 min on an Intel Xeon 2.4 GHz workstation with a 32.0 GB RAM.

4.2. Model validation

The model is developed under the experimental operating condition that are derived from Ref. [28], and its structure is shown in Fig. 5. The geometric parameters of the model are listed in Table 4. The comparison of the results of the model and experimental data is shown in Fig. 7. It is observed that there is only a small difference between the results of the model and experimental data. The model is validated to be a reliable model for the optimization of the channel structure.

4.3. The multi-objective optimization

The optimal operating conditions obtained in Section 3 are applied to the numerical model described above. Then, the channel structure of the PEMFC is optimized by a multi-objective optimization method. Here, multi-objective optimization method is a combination of numerical simulation and genetic algorithm [30,31]. This type of method is efficient and reliable for finding the optimal structure of a PEMFC channel.

As shown in Fig. 5, the height of the channel inlet, *a*, and height of the channel outlet, *b*, are chosen to be variables of the optimiza-

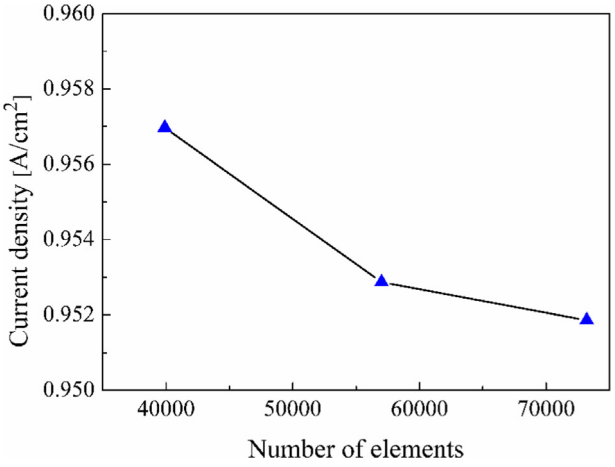

Fig. 6. Grid independent test.

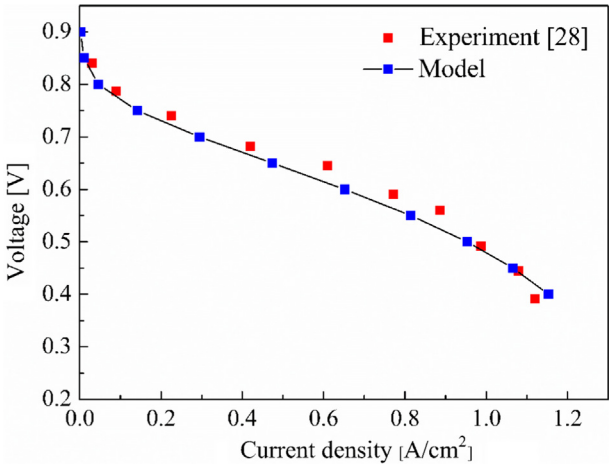

Fig. 7. Polarization curve: comparison of simulations and experiment.

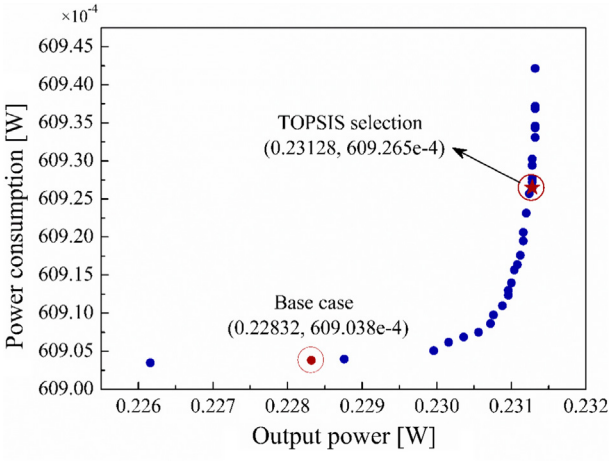

Fig. 8. Pareto front of channel optimization.

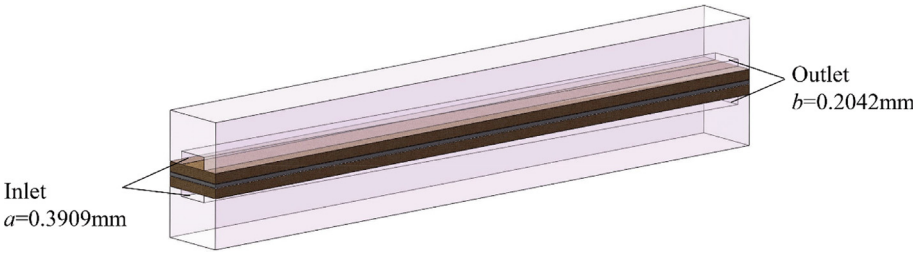

Fig. 9. Geometric structure of the optimal case.

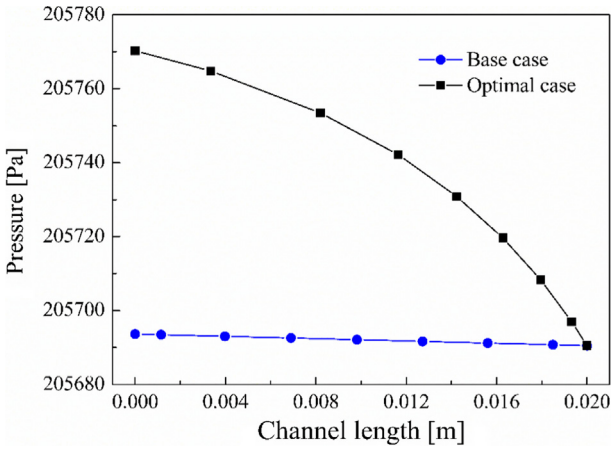

Fig. 10. Pressure along the channel of the base case and optimal case.

tion process. Additionally, the output power and power consumption of the fuel cell are the optimization objectives. The multi-objective optimization method is the same as the method that used in the multi-objective optimization of the stack mentioned above. The optimization is described by following mathematic model.

$$\min[-E_{cell}, E_{con}] \tag{36}$$

s.t.

$$0.2 \leqslant a \leqslant 1.3 \text{ mm}$$

$$0.2 \leqslant b \leqslant 1.3 \text{ mm}$$

where E_{cell} is the output power and E_{con} is the power consumption of fuel cell. The power consumption of the fuel cell is considered as the power consumption of the air compressor. The expressions of the output power and power consumption of the air compressor are shown as follows.

$$E_{cell} = V_{cell} I A \tag{37}$$

$$E_{con} = P_{c\_in} U_{c\_in} A_{ch\_in} \tag{38}$$

In Eq. (37), V_{cell}, I and A are the voltage, current density and active area of the fuel cell, respectively. The current density, I, is 0.89 A/cm^2 derived from the optimal operating condition. In Eq. (37), P_{c_in}, U_{c_in} and A_{ch_in} are the pressure, velocity, and area of the channel inlet, respectively.

4.4. Result and discussion of the channel optimization

After the calculation under the optimal operating condition, a series of optimal solutions are obtained as shown in Fig. 8. From these optimal solutions, one solution is selected by TOPSIS. The selected optimal solution is used as the optimal case. The output power and power consumption of optimal case are 0.23128 W and 609.265e−4 W, respectively. For the base case, using the geometric parameters shown in Table 5, the output power and power consumption are 0.22832 W and 609.038e−4 W, respectively. Compared with the base case, the power consumption of the optimal case increased by 0.373% while the output power increased by 1.296%. The increment of the output power is larger than that of the power consumption.

As shown in Fig. 9, the height of the channel inlet a and height of the channel outlet b for the optimal case are 0.3909 mm and 0.2042 mm, respectively. Compared with the channel of the base case, the channel of the optimal case is smaller and tapered. This type of channel results in a higher pressure drop. As shown in Fig. 10, the pressure drop of the optimal case is 79.73 Pa and the pressure drop of the base case is 3.14 Pa. The pressure of the optimal case is higher than that of the base case from the inlet to outlet. At the interface between the channel and gas diffusion layer, the average pressure of the base case is 205,672 Pa and the average pressure of the optimal case is 205,742 Pa. The higher pressure of the optimal case provides for better mass transfer performance of the fuel cell.

In Fig. 11(a), the contour planes are used to describe the molar concentration of the oxygen in the cathode side for both the base and optimal cases. As can be seen, the distribution of oxygen for the optimal case is more uniform. This can be explained by the higher pressure of optimal case forcing oxygen to diffuse to the gas diffusion layer. In Fig. 11(b), the molar concentration of oxygen at the interface between the gas diffusion layer and catalyst layer for the base case and optimal case is shown. It can then be determined that the oxygen concentration of the optimal case is higher. The average oxygen concentrations of the base case and optimal cases are 7.0309 mol/m^3 and 8.1126 mol/m^3, respectively. This means that more oxygen is transported to the surface of the catalyst layer for the optimal case and more oxygen participates in the electrochemical reaction in the catalyst layer. Therefore, the optimal channel structure improves the performance of mass transfer in the PEMFC. As a result, the output performance of the PEMFC is improved.

In Fig. 12, the polar curves of the base case and optimal case are shown. Here we compare the output performance of these two cases under different operating voltages. It can be seen that the output performance of the optimal case is better than that of the base case, especially at low voltage. When the operating voltage is 0.5 V, the current density of the base case is 1.3701 A/cm^2 and the current density of the optimal case is 1.4762 A/cm^2. Compared with base case, the optimal case increases the current density by 7.7%. When the voltage is 0.4 V, the current density of the optimal case increases by 9.54%.

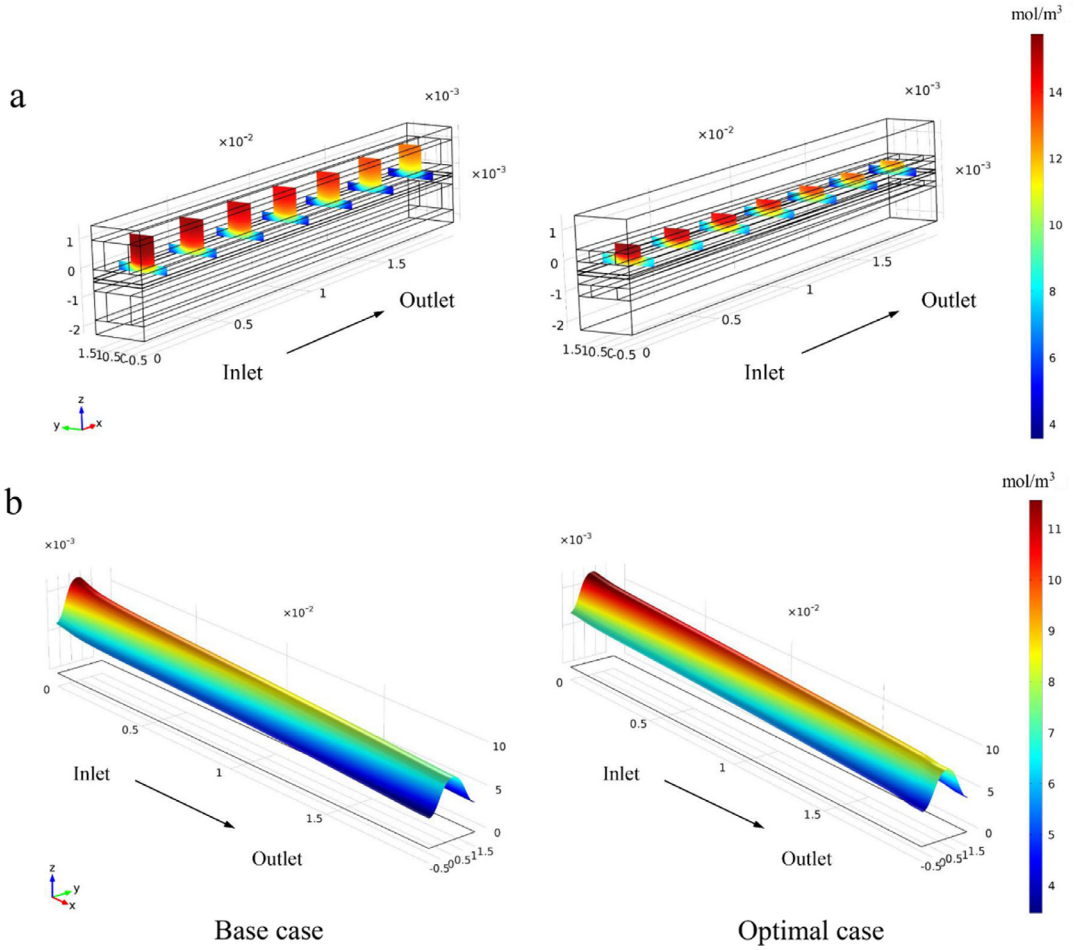

Fig. 11. Comparison of oxygen concentration: (a) oxygen distribution from the inlet to outlet, and (b) oxygen at the interface between the gas diffusion layer and catalyst layer.

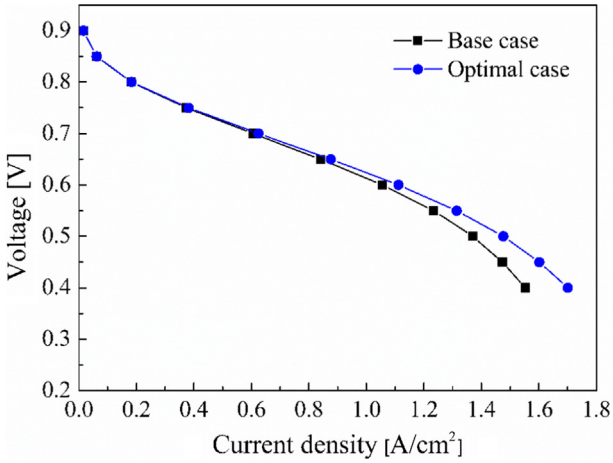

Fig. 12. Polar curve of base case and optimal case.

5. Conclusion

In this work, we optimized the operating condition and channel structure of PEMFC. A PEMFC stack model was established for the optimization of operating condition. The multi-objective genetic algorithm was then applied to optimize the operating condition. The variables of the optimization included temperature, anode pressure, cathode pressure, and operating current density. The objectives of the optimization process were energy efficiency and output power. The optimal result was chosen by TOPSIS from the Pareto front. The optimal temperature, anode pressure, cathode pressure, and operating current density were 366.15 K, 4.99 atm, 3.02 atm, and 0.89 A/cm^2, respectively.

We then optimized the channel structure of the PEMFC by using the multi-objective genetic algorithm based on the optimal operating condition. The variables of the optimization process were the heights of channel inlet and channel outlet and the objectives were the power consumption and output power of the PEMFC. The optimal channel obtained by optimization was a tapered channel whose height at the inlet and outlet are 0.3909 mm and 0.2042 mm, respectively. The optimal channel provided a higher pressure to the mass transfer of fuel cell. This subsequently enhanced the performance of mass transfer. As a result, the output performance of PEMFC was improved.

The optimizations in this paper for the operating condition and channel structure of PEMFC by multi-objective genetic algorithm could be applied to guide the design of PEMFC. For a PEMFC, combining the multi-objective genetic algorithm, TOPSIS selection and numerical simulation is an effective method for finding the optimal operating condition and channel structure.

Acknowledgements

The work is supported by the National Natural Science Foundation of China (51376069) and the National Key Basic Research Program of China (973 Program) (2013CB228302).

References

[1] X.D. Wang, W.M. Yan, Y.Y. Duan, et al., Numerical study on channel size effect for proton exchange membrane fuel cell with serpentine flow field, Energy Convers. Manage. 51 (5) (2010) 959–968.

[2] A. Raj, T. Shamim, Investigation of the effect of multidimensionality in PEM fuel cells, Energy Convers. Manage. 86 (2014) 443–452.

[3] G. Hu, G. Li, Y. Zheng, et al., Optimization and parametric analysis of PEMFC based on an agglomerate model for catalyst layer, J. Energy Inst. 87 (2) (2014) 163–174.

[4] W. Na, B. Gou, The efficient and economic design of PEM fuel cell systems by multi-objective optimization, J. Power Sources 166 (2) (2007) 411–418.

[5] S.M.C. Ang, D.J.L. Brett, E.S. Fraga, A multi-objective optimisation model for a general polymer electrolyte membrane fuel cell system, J. Power Sources 195 (9) (2010) 2754–2763.

[6] S.O. Mert, I. Dincer, Z. Ozcelik, Exergoeconomic analysis of a vehicular PEM fuel cell system, J. Power Sources 165 (1) (2007) 244–252.

[7] J. Wishart, Z. Dong, M. Secanell, Optimization of a PEM fuel cell system based on empirical data and a generalized electrochemical semi-empirical model, J. Power Sources 161 (2) (2006) 1041–1055.

[8] S.O. Mert, I. Dincer, Z. Ozcelik, Performance investigation of a transportation PEM fuel cell system, Int. J. Hydrogen Energy 37 (1) (2012) 623–633.

[9] K. Jiao, J. Bachman, Y. Zhou, et al., Effect of induced cross flow on flow pattern and performance of proton exchange membrane fuel cell, Appl. Energy 115 (2014) 75–82.

[10] Z. Wan, J. Shen, H. Zhang, et al., In situ temperature measurement in a 5kW-class Proton Exchange Membrane Fuel Cell stack with pure oxygen as the oxidant, Int. J. Heat Mass Transfer 75 (2014) 231–234.

[11] H. Pei, Z. Liu, H. Zhang, et al., In situ measurement of temperature distribution in proton exchange membrane fuel cell I a hydrogen–air stack, J. Power Sources 227 (2013) 72–79.

[12] Z. Liu, J. Shen, H. Pei, et al., Effect of humidified water vapor on heat balance management in a proton exchange membrane fuel cell stack, Int. J. Energy Res. 39 (4) (2015) 504–515.

[13] L. Matamoros, D. Brüggemann, Simulation of the water and heat management in proton exchange membrane fuel cells, J. Power Sources 161 (1) (2006) 203–213.

[14] S.W. Perng, H.W. Wu, T.C. Jue, et al., Numerical predictions of a PEM fuel cell performance enhancement by a rectangular cylinder installed transversely in the flow channel, Appl. Energy 86 (9) (2009) 1541–1554.

[15] A.P. Manso, F.F. Marzo, M.G. Mujika, et al., Numerical analysis of the influence of the channel cross-section aspect ratio on the performance of a PEM fuel cell with serpentine flow field design, Int. J. Hydrogen Energy 36 (11) (2011) 6795–6808.

[16] M. Bilgili, M. Bosomoiu, G. Tsotridis, Gas flow field with obstacles for PEM fuel cells at different operating conditions, Int. J. Hydrogen Energy 40 (5) (2015) 2303–2311.

[17] W.J. Yang, H.Y. Wang, Y.B. Kim, Channel geometry optimization using a 2D fuel cell model and its verification for a polymer electrolyte membrane fuel cell, Int. J. Hydrogen Energy 39 (17) (2014) 9430–9439.

[18] H.C. Chiu, J.H. Jang, W.M. Yan, et al., A three-dimensional modeling of transport phenomena of proton exchange membrane fuel cells with various flow fields, Appl. Energy 96 (2012) 359–370.

[19] S.W. Perng, H.W. Wu, Non-isothermal transport phenomenon and cell performance of a cathodic PEM fuel cell with a baffle plate in a tapered channel, Appl. Energy 88 (1) (2011) 52–67.

[20] D.H. Ahmed, H.J. Sung, Effects of channel geometrical configuration and shoulder width on PEMFC performance at high current density, J. Power Sources 162 (1) (2006) 327–339.

[21] S.W. Perng, H.W. Wu, R.H. Wang, Effect of modified flow field on non-isothermal transport characteristics and cell performance of a PEMFC, Energy Convers. Manage. 80 (2014) 87–96.

[22] J.K. Kuo, T.S. Yen, Improvement of performance of gas flow channel in PEM fuel cells, Energy Convers. Manage. 49 (10) (2008) 2776–2787.

[23] J.Y. Jang, C.H. Cheng, Y.X. Huang, Optimal design of baffles locations with interdigitated flow channels of a centimeter-scale proton exchange membrane fuel cell, Int. J. Heat Mass Transfer 53 (4) (2010) 732–743.

[24] É. Fontana, E. Mancusi, A. Da Silva, et al., Study of the effects of flow channel with non-uniform cross-sectional area on PEMFC species and heat transfer, Int. J. Heat Mass Transfer 54 (21) (2011) 4462–4472.

[25] N. Pourmahmoud, H. Sadeghifar, A. Torkavannejad, A novel, state-of-the-art tubular architecture for polymer electrolyte membrane fuel cells: performance enhancement, size and cost reduction, Int. J. Heat Mass Transfer 108 (2017) 577–584.

[26] X. Zeng, Y. Ge, J. Shen, et al., The optimization of channels for a proton exchange membrane fuel cell applying genetic algorithm, Int. J. Heat Mass Transfer 105 (2017) 81–89.

[27] L. Zhang, N. Wang, An adaptive RNA genetic algorithm for modeling of proton exchange membrane fuel cells, Int. J. Hydrogen Energy 38 (1) (2013) 219–228.

[28] L. Wang, A. Husar, T. Zhou, et al., A parametric study of PEM fuel cell performances, Int. J. Hydrogen Energy 28 (11) (2003) 1263–1272.

[29] S.O. Mert, Z. Özçelik, Y. Özçelik, et al., Multi-objective optimization of a vehicular PEM fuel cell system, Appl. Therm. Eng. 31 (13) (2011) 2171–2176.

[30] Y. Ge, Z. Liu, W. Liu, et al., Active optimization design theory and method for heat transfer unit and its application on shape design of cylinder in convective heat transfer, Int. J. Heat Mass Transfer 90 (2015) 702–709.

[31] Y. Ge, Z. Liu, W. Liu, Multi-objective genetic optimization of the heat transfer for tube inserted with porous media, Int. J. Heat Mass Transfer 101 (2016) 981–987.